Effect of Fe on microstructure and properties of 8xxx aluminum conductor alloys

Lei Pan[1*], Kun Liu[1], Francis Breton[2] and X.-Grant Chen[1]

[1] Department of Applied Science, University of Québec at Chicoutimi

Saguenay (QC), Canada, G7H 2B1

[2] Arvida Research and Development Centre, Rio Tinto, Saguenay (QC), Canada, G7S 4K8

*Corresponding author: Tel.: 1 418 545 5011 # 7109; Fax: 1 418 545 5012; E-mail: lei.pan1@uqac.ca

Abstract

The effect of Fe contents (0.3−0.7 wt.%) on the microstructure, electrical conductivity, mechanical and creep properties of 8xxx aluminum conductor alloys was investigated. Results revealed that the as-cast microstructure of 8xxx alloys was consisted of equiaxed α-Al grains and secondary Fe-rich intermetallics distributed in the interdendritic region. The extruded microstructure showed partially recrystallized structure for 0.3% Fe alloy but only dynamically recovered structures for 0.5% and 0.7% Fe alloys. With increasing Fe contents, the ultimate tensile strength and yield strength were remarkably improved while the electrical conductivity was slightly decreased. Moreover, the creep resistance was greatly improved, which is attributed to the larger volume fraction of fine intermetallic particles and smaller subgrain size in the higher Fe-containing alloys. The creep threshold stress was found to increase from 24.6 to 33.9 MPa with increasing Fe contents from 0.3% to 0.7%, respectively. The true stress exponent values were close to 3 for all three experimental alloys, indicating that the creep

mechanism of 8xxx alloys was controlled by dislocation glide.

Keywords: 8xxx electrical conductor alloys; Fe content; Electrical conductivity; Mechanical properties; Creep resistance.

1. Introduction

Due to the low density and high conductivity to weight ratio, aluminum conductor alloys become an attractive candidate for replacing copper electric conductors in power building wiring (Ref 1-3). Among those, 8xxx aluminum alloys are one of the most widely used aluminum conductor alloys, which were firstly developed to replace AA1350 conductor alloys for the overhead electrical transmission (Ref 4). For conductor alloys, it is necessary to satisfy the requirements for electrical conductivity (EC), strength and creep resistance (Ref 5, 6). Fe is added in this alloy as the main alloying element to improve microstructural stability and mechanical properties (Ref 7, 8). Because of the low solubility of Fe in Al (Ref 9), most of Fe combines with both aluminum and silicon to form secondary intermetallic particles during casting, such as Al_3Fe, Al_mFe, Al_6Fe, and α-AlFeSi (Ref 10-12). In the fabrication processes of aluminum electric conductors, the supply rods (9.53 mm in diameter) prior to wire drawing were either conventionally cast and hot-rolled or produced by continuous cast-rolling operation (Propezi process). During hot deformation the Fe-rich intermetallic particles were broken up into segments and distributed as fine dispersoids in aluminum matrix (Ref 13, 14). Addition of Fe is reported to play an important role in the hot deformation behavior (Ref 14, 15). However, little

investigations have been conducted on the effect of Fe on the microstructure evolution and their consequent inference on materials properties of aluminum conductor alloys.

The creep resistance is one of the most important properties in aluminum conductor alloys (Ref 16-18). To ensure high reliability in any further application of aluminum conductors, it is necessary to understand the effect of Fe on the creep behavior of aluminum conductor alloys. However, there have been controversial observations about effect of Fe on creep properties. Westerlund (Ref 16) found that addition of 0.65 wt.% Fe to Al−Fe alloy resulted in a significant reduction of the creep resistance. But, McQueen *et al*. (Ref 7) investigated the effect of Fe-rich intermetallic particles on the aluminum conductors and showed that addition of Fe could greatly improve the creep resistance for Al−Fe alloys (0.5−0.65 wt.% Fe). Up to day, limited data are available on the effect of Fe contents on the creep properties in 8xxx alloys at the common operating temperatures (up to ~100°C) in the open literature, which is an important concern for their applications in the electric conductor industry.

The present work, therefore, aimed to investigate the effect of Fe contents on the evolution of microstructure, electrical conductivity, and mechanical and creep properties in 8xxx aluminum conductor alloys. The conventionally extruded 8xxx aluminum alloy conductors with different Fe contents were subjected to the compression creep test at 100°C. The creep mechanism based on the creep threshold stress and true stress exponent is also explored to better understand the creep resistance in 8xxx aluminum conductor alloys.

2. Experimental

The experiments were conducted on 8xxx Al alloys with different Fe contents ranging from 0.3% to 0.7% (all alloy compositions in this work are in wt.% unless otherwise indicated). The chemical compositions of experimental alloys analyzed with an optical emission spectrometer are listed in Table 1. All the samples (equivalent to the industrial 9.53 mm supply rods for drawn wire) were produced by the hot extrusion from DC cast billets.

The electrical conductivity measurement was directly carried out on the samples of 9.53 mm in diameter and 200 mm in length using Megger DLRO10HD resistance ohmmeter. Tensile tests were conducted on cylindrical samples of 9.53 mm in diameter and 250 mm long according to ASTM B557 standard at room temperature. The compressive creep tests were performed at 100°C using cylindrical specimens (9.5 mm in diameter and 19 mm in length) under a constant stress that varied between 35 and 69 MPa. After the creep test, the samples were water quenched to the room temperature to examine the microstructure evolution.

The as-cast and extruded samples were polished and etched by the Keller's solution for 10 s, and then observed using optical microscope (OM), scanning electron microscope (SEM) and electron backscattered diffraction (EBSD) technique. All the extruded samples were sectioned parallel to the extrusion direction along the centerline and followed by the standard metallographic preparation. The automated EBSD maps were conducted with 1.0 μm step size for as-cast grain structure and with a scanning step size of 0.2 μm for the extruded structure. The subgain sizes of the extruded samples were measured using linear intercept method (Ref 19). In addition, the samples after creep tests at 69 MPa

and 100°C were selected to investigate the microstructure evolution using transmission electron microscope (TEM), which was operated at 200 kV. TEM samples with a thickness of 35−60 μm were prepared by mechanically grounding and electropolishing in a solution of 30% nitric acid and 70% methanol at 15 V and −20°C.

3. Results and discussion

3.1 Microstructures of as-cast and extruded materials

Figure 1 shows the optical micrographs of as-cast 8xxx aluminum alloys prior to hot extrusion with different Fe contents (0.3%, 0.5% and 0.7%). All the alloys had similar microstructure that is consisted of equiaxed α-Al grains and secondary Fe-rich intermetallics distributed in the interdendritic region (Fig. 1). It can be seen that the amount of the intermetallic phase increases with increasing Fe contents. As shown in Fig. 2, the appearance of the intermetallic phase (arrows in Fig. 1) is feathery-like Al−Fe phase, confirmed by SEM-EDS (Fig. 2b). Those intermetallics are identified as body-centered-tetragonal Al_mFe phase by EBSD results (Fig. 2c and 2d) with lattice parameters a=0.884 nm and c=2.160 nm (Ref. DOI: 10.1007/s11661-011-1004-5). In previous study (Ref 14, 16), these intermetallics were identified as Al_6Fe or Al_3Fe phase, which was only based on SEM-EDS qualitative results. The as-cast grain structure is refined due to the restriction effect of intermetallic particles. The average gain sizes measured by EBSD are 86, 77 and 71 μm for the alloys containing 0.3%, 0.5% and 0.7% Fe, respectively.

Figure 3 shows the optical images of the extruded samples. The hot extrusion fragmented and

broke down intermetallic networks into fine particles which distributed along the extrusion direction in the aluminum matrix. For all the alloys, the Fe-rich intermetallic particles in extruded samples were small and fairly uniformly distributed throughout the matrix. The average size of intermetallic particles was measured to be a similar value of ~0.38 μm for all three alloy samples. However, the volume fraction of intermetallic particles is increased from 1.9% in Al3 alloy to 3.2% in Al5 alloy and further to 4.4% in Al7 alloy, respectively.

Figure 4 shows the EBSD orientation maps of extruded samples of Al3, Al5 and Al7 alloys. In the orientation imaging maps, the boundaries of grains and subgrains are defined as follows: white lines: 1−5°, blue lines: 5−15°, thin black lines: 15−30° and thick black lines: (> 30°). When the DC cast billets were extruded to the rods, the original grains of three alloys were severely torn and broke into the irregular deformation bands along the elongated grains. A large amount of low-angle boundaries with misorientation angles between of 1° and 5° were created, indicating a high number density of subgrain structure. Meanwhile, the substructures were well organized and fine subgrains were formed with neatly arranged boundaries of 1−15°, which suggests the dynamic recovery occurred, involving the annihilation and rearrangement of dislocations (Ref 20). For Al3 alloy as indicated by arrows in Fig. 4a, small equiaxed grains with high-angle boundaries (> 15°) that contained substructures were observed along the elongated grain boundaries, indicating partially dynamic recrystallization occurred during extrusion. However, only dynamically recovery was observed in the alloys containing 0.5% and 0.7% Fe (Fig. 4b and c), which was resulted from the inhabitation effect of high volume fraction of Fe-rich intermetallic particles on dynamic recrystallization. As measured from EBSD orientation maps (Fig. 4), the average subgrain sizes decreased from 3.9, 3.2 to 2.8 μm as the Fe content increased from

0.3% to 0.5% and further to 0.7%, respectively. The increased volume fraction of Fe-rich intermetallic particles in alloys containing high Fe generated a stronger pinning effect on substructures and led to a decrease in subgrain size (Ref 15).

3.2 Effect of Fe on mechanical and electrical properties

Figure 5 shows the evolution of ultimate tensile strength (UTS), yield strength (YS), elongation and electrical conductivity (EC) with different Fe contents. It can be found that both UTS and YS increase while the elongation barely changes with increasing Fe contents from 0.3% to 0.7% (Fig. 5a). The UTS and YS of Al3 alloy are 108 MPa and 91 MPa, respectively. As the Fe contents increase to 0.5% and 0.7%, the UTS and YS increase approximately by 8% and 10% for Al5 alloy and 25% and 28% for Al7 alloy, respectively. Meanwhile, the EC of samples moderately decreases with an increase of Fe content (Fig. 5b). The EC of Al3 alloy is 61.1 % IACS and it decreases to 60.5% for Al5 alloy and 59.7% for Al7 alloy, respectively.

In the extruded samples, there were a large number of Fe-rich intermetallic particles with an average size of 0.38 μm present (Fig. 3). With increase of Fe contents, the volume fraction of Fe-rich intermetallic particles increases and those particles can act as obstacles to the movement of dislocation and block of the migration of grain boundaries, leading to the improvement of both UTS and YS. Besides the intermetallic particles, with increase of Fe contents the recrystallization grains disappeared and the subgrains became smaller (Fig. 4), which provided more obstacles for dislocation motion and thus improved tensile properties. On the other hand, the intermetallic particles present in aluminum

matrix created a number of defects in the crystal structure. Those intermetallic particles and its related crystal defects hindered the free movement of electrons, resulting in a decrease in the electrical conductivity with an increase of Fe contents.

In the industrial practice, the annealing after wire drawing is often used to improve the electrical conductivity of conductor products. Figure 6 shows the mechanical properties and EC after annealing treatment at 350 ºC for 4 h for three different Fe contained alloys. It is noted the EC increases more than 1% for all three alloys compared to that before annealing and their values are 62.0 % IACS for Al3 alloy, 61.7% for Al5 alloy and 61.1% for Al7 alloy, respectively. For some critical applications where EC is the primary concern, even with higher Fe contents, both Al5 and Al7 alloys can fulfill the minimum requirement (EC ≥ 61.0 % IACS). However, The UTS and YS considerably decrease after annealing for all three alloys. There is a trade-off between the strength and EC when the annealing process is applied.

3.3 Effect of Fe on creep properties

Figure 7 shows typical creep curves of extruded Al3, Al5 and Al7 samples tested at 100 °C under a constant stress of 69 MPa, which is close to the compressive YS at 100°C (73 MPa of Al3 alloy). It can be clearly seen from Fig. 7a that the total stain after 200 h test decreases from the low Fe alloy (Al3) to the high Fe alloy (Al7). In compressive creep tests, the creep strain increases rapidly at the beginning of the creep deformation, which can be defined as the primary creep stage where the creep rate dramatically decreased with creep time. The creep stain then rises more slowly with increasing time and the primary creep stage gradually transits to a stage where the creep rate becomes more and less

constant (quasi-steady stage). As indicated in Fig. 7b, the minimum creep rate, $\dot{\varepsilon}_m$, is calculated as the average creep rate in the quasi-steady stage, and the results demonstrate that with increasing Fe content from 0.3% to 0.7%, the minimum creep rate significantly decreases from $7.5 \times 10^{-8}\ s^{-1}$ (Al3 alloy) to $1.8 \times 10^{-8}\ s^{-1}$ (Al5 alloy) and further to $5.6 \times 10^{-9}\ s^{-1}$ (Al7 alloy), respectively, indicating a strong benefit of Fe on improving the creep resistance.

To further understand the creep behavior of 8xxx conductor alloys, various loads in the range of 35−69 MPa were applied for the creep tests at the same temperature (100°C). Figure 8 shows the minimum creep rate, $\dot{\varepsilon}_m$, as a function of the applied stress for three alloys. It is apparent that at any given stress, the minimum creep rate remarkably decreased from Al3 alloy to Al7 alloy. In other words, the creep resistance of 8xxx conductor alloys clearly increases with increasing Fe contents. By extrapolating the linear fitted curves to the creep rate value of $10^{-10}\ s^{-1}$, the threshold stress, σ_{th}, below which creep is not experimentally measurable, can be determined for each alloy. The values of threshold stresses are calculated to be 24.6 MPa (Al3 alloy), 30.1 MPa (Al5 alloy) and 33.9 MPa (Al7 alloy), respectively (Fig. 8). It is evident that the creep threshold stress increases with increasing Fe contents. The origin of the threshold stress in dispersion strengthened alloys is assumed to be the interaction between the dislocations and dispersion particles. The common explanation for σ_{th} is the presence of an additional stress to bow the dislocation between the particles, corresponding Orowan stress (Ref 21). Arzt *et al*. (Ref 22, 23) considered that the threshold stress was the stress required to detach a dislocation from an obstacle or the additional stress required for climbing over an obstacle.

After determining the threshold stress, the creep behavior of dispersion strengthened materials can be generally described by a modified power law equation as follows (Ref 24):

$$\dot{\varepsilon}_{\mathrm{m}} = A_0 \left(\frac{\sigma-\sigma_{\mathrm{th}}}{G}\right)^{n_{\mathrm{t}}} \exp\left(-\frac{Q}{RT}\right) \quad (1)$$

where $\dot{\varepsilon}_{\mathrm{m}}$ is the minimum creep rate, A_0 is a dimensionless constant, G is the shear modulus; n_t is the true stress exponent, Q is the activation energy, R is the universal gas constant and T is the absolute temperature, σ is the applied stress and σ_{th} is the threshold stress. Figure 9 shows the double logarithmic plot of the minimum creep rate, $\dot{\varepsilon}_{\mathrm{m}}$, over the effective stress, $\sigma-\sigma_{th}$, and the slope of plots gives the true stress exponent n_t. It can be found that the values of n_t are in a range of 2.5−3.3 for three alloys with different Fe contents, which can be used to assess the mechanisms governing creep deformation. The creep behavior of aluminum alloys related to three relevant deformation mechanisms are the dislocation glide (n_t = 3), dislocation climb (n_t = 5) and invariant substructure model (n_t = 8) (Ref 25-27). In the present study, the values of the true stress exponent, n_t, are close to 3, indicating that the creep process is controlled by dislocation glide, which is also confirmed by Jaffe and Dorn that dislocation glide mechanism was responsible for room temperature creep in pure aluminum (Ref 28, 29).

Though the creep properties vary with Fe contents, as shown in Figs. 7 and 8, however, the creep behaviours are confirmed to be controlled by the dislocation glide for all experimental Al3, Al5 and Al7 alloys with a similar n_t in Fig. 9. Therefore, the factors that can have effect on the movement of dislocations during creep are expected to influence the creep properties, which principally are the fine intermetallic particles and subgrains in the present work. It is observed that dislocations are piled-up at intermetallic particles, as shown in Fig. 10a, confirming the inhibiting effect of intermetallic particles on dislocations and their influence on creep properties. Besides, the threshold stress originates from the dislocation looping over the particles (Orowan stress, σ_{or}) can be evaluated from Eq. 2 (Ref 21, 24):

$$\sigma_{or} = 0.84M\frac{Gb}{d}(\sqrt{\frac{\pi}{4f}} - 2)^{-1} \quad (2)$$

where M is Taylor factor with the value of 3.06 (Ref. 24), G is the Gibbs free energy, which is 24.4 GPa at 100°C (Ref. 24) d is average particle diameter and it is calculated to be about 0.368 um for all Fe contents studied in the present work, and f is the particle volume fraction. In the present work, the particle volume fractions f, are 1.9% in Al3 alloy, 3.2% in Al5 alloy and 4.4% in Al7 alloy, respectively (Fig. 3). Hence, the Orowan stress σ_{or} has been calculated to be 10.7 MPa in Al3, 16.0 MPa in Al5, and 21.2 MPa in Al7 alloys, respectively. It is apparent that the increased volume fraction of intermetallic particles (f) results in the rising σ_{or} due to the increment in the interaction between fine particles and dislocations.

However, the calculated values, σ_{or}, are smaller than the experimentally determined values, σ_{th}, (Fig. 8). This could be likely attributed to the synergy effect of other minor and trace elements (such as Cu, Si) in aluminum matrix, which can also contribute to the part of σ_{th} (Ref 30, 31). In addition, the effect of solute atoms should be same due to a similar solution level of solute atoms in all three experimental alloys, which can be confirmed by the liner fit between σ_{th} and σ_{or} in Fig. 11. Therefore, with increasing Fe contents, the volume fraction of intermetallic particles rises, which leads to increasing the Orowan stress, σ_{or} and experimental stress σ_{th}, resulting in a significant improvement of the creep resistance.

In addition, as shown in Fig. 10b, entangled dislocations interacted with subgrain boundaries and became immobilized, suggesting the beneficial effect of subgrains on the creep resistance. At relatively high temperature (> 0.5 T_m), subgrain boundaries are generally considered to be harmful to the creep properties due to their unstable and easily-sliding features during creep. However, the creep test

temperature is relatively low ($\approx< 0.4\ T_m$) in the present study and the dislocation glide controls the creep deformation (Fig. 9), indicating an absence of subgrain boundaries sliding (Ref 32), which is further confirmed by the TEM observation. Fig. 10b illustrates that the subgrain boundary can also act as barriers for dislocation motion during creep deformation and Fig. 10c shows that a large part of the intermetallic particles distribute on the subgrain boundaries, which increases the pining effect on subgrain boundaries and hence enhances the subgrain stability. Thus, the presence of fine subgrains results in a positive strengthening effect on creep properties. As demonstrated in Fig. 4, the subgrain size decreased with increasing Fe contents, which reduces the mean free path for dislocation movement and generates an additional contribution to a better creep resistance.

4. Conclusions

The effects of Fe contents on microstructure and properties of 8xxx aluminum conductor alloys were investigated. The following conclusions can be drawn:

1. The as-cast microstructure of 8xxx alloys was consisted of equiaxed α-Al grains and secondary Fe-rich intermetallics distributed in the interdendritic region. The deformed microstructure showed partially recrystallized structure for 0.3% Fe alloy but only dynamically recovered structures for 0.5% and 0.7% Fe alloys. The volume fraction of fine intermetallic particles increased and the subgrain size decreased after hot deformation with increasing Fe contents.
2. As the amount of Fe increased from 0.3% to 0.7%, UTS and YS increased by 25% and 28% while EC decreased by 2.3%, respectively. After annealing at 350ºC for 4 h, EC increased more than 1%

for all three alloys compared to that before annealing alloy in the trade-off with reduced tensile strength.

3. Addition of Fe to 8xxx alloys greatly improved the creep resistance. With increase of Fe content from 0.3% to 0.5% and 0.7%, the minimum creep rate significantly decreased from $7.5 \times 10^{-8}\ s^{-1}$ to $1.8 \times 10^{-8}\ s^{-1}$ and further to $5.6 \times 10^{-9}\ s^{-1}$, respectively, for creep tests at 100°C with a constant stress of 69 MPa.
4. With increasing Fe contents from 0.3% to 0.5% and 0.7%, the creep threshold stress greatly increased from 24.6 to 30.1 and 33.9 MPa, respectively.
5. The introduction of the threshold stress in the analysis resulted in that the true stress exponent values were close to 3 for all three experimental alloys, indicating that the creep mechanism of 8xxx alloys is controlled by dislocation glide. The presence of larger volume fraction of fine intermatllic particles and smaller subgrain size in the higher Fe-containing alloys are responsible for the better creep resistance.

Acknowledgments

The authors would like to acknowledge financial support from Natural Science and Engineering Research Council of Canada (NSERC) and Rio Tinto through the NSERC Industrial Research Chair in Metallurgy of Aluminum Transformation at the University of Quebec at Chicoutimi.

References

[1] M.Y. Murashkin, I. Sabirov, X. Sauvage, R.Z. Valiev, Nanostructured Al and Cu alloys with superior strength and electrical conductivity, J. Mater Sci, 2016, 51(1), p 33-49.
[2] W.H. Yuan, Z.Y. Liang, Effect of Zr addition on properties of Al-Mg-Si aluminum alloy used for all aluminum alloy conductor, Mater. Des., 2011, 32(8-9), p 4195-4200.
[3] L. Pan, B. Bourassa, X.G. Chen, Effect of thermomechanical processing on electrical and mechanical properties of aluminum conductor alloys, Materials Science Forum, 2014, 794-796, p 1121-1126.
[4] C. Olin, Aluminum alloy conductor, in: U.S.P. 3711339 (Ed.) US, 1973.
[5] X.K. Ji, H. Zhang, S. Luo, F.L. Jiang, D.F. Fu, Microstructures and properties of Al-Mg-Si alloy overhead conductor by horizontal continuous casting and continuous extrusion forming process, Mater. Sci. Eng. A, 2016, 649, p 128-134.
[6] K.W. Barber, K.J. Callaghan, Improved overhead line conductors using aluminum alloy 1120, IEEE T. P. Deliver, 1995, 10(1), p 403-409.
[7] H.J. Mcqueen, E.H. Chia, E.A. Starke, Fe-particle-stabilized Aluminum conductors, JOM, 1986, 38(4), p 19-24.
[8] X.Y. Zhang, H. Zhang, X.X. Kong, D.F. Fu, Microstructure and properties of Al-0.70Fe-0.24Cu alloy conductor prepared by horizontal continuous casting and subsequent continuous extrusion forming, Trans. Nonferrous Met. Soc. China, 2015, 25(6), p 1763-1769.
[9] O.D. Sherby, A. Goldberg, O.A. Ruano, Solute-diffusion-controlled dislocation creep in pure aluminium containing 0.026 at.% Fe, Philos. Mag., 2004, 84(23), p 2417-2434.
[10] P. Skjerpe, Intermetallic phases formed during DC-casting of an Al-0.25 Wt Pct Fe-0.13 Wt Pct Si alloy, Metall. Trans. A, 1987, 18(2), p 189-200.
[11] C.M. Allen, K.A.Q. O'Reilly, B. Cantor, P.V. Evans, Intermetallic phase selection in 1XXX Al alloys, Prog. Mater. Sci., 1998, 43(2), p 89-170.
[12] M. Shakiba, N. Parson, X.G. Chen, Effect of homogenization treatment and silicon content on the microstructure and hot workability of dilute Al-Fe-Si alloys, Mater. Sci. Eng. A, 2014, 619, p 180-189.
[13] D. Kalish, B.G. Lefevre, S.K. Varma, Effect of alloying and processing on subgrain-strenth relationship in aluminum conductor alloys, Metall. Mater. Trans. A, 1977, 8(1), p 204-206.
[14] H.J. Mcqueen, K. Conrod, G. Avramovic-cingara, The hot-working characteristics of eutectic-rod-stabilized conductor alloys, Can. Metall. Quart., 1993, 32(4), p 375-386.
[15] M. Shakiba, N. Parson, X.G. Chen, Effect of iron and silicon content on the hot compressive deformation behavior of dilute Al-Fe-Si alloys, J. Mater. Eng. Perform., 2015, 24(1), p 404-415.
[16] R.W. Westerlund, Effects of composition and fabrication practice on resistance to annealing and creep of aluminum conductor alloys, Metall. Trans., 1974, 5(3), p 667-672.
[17] D.E. Newbury, What Is Causing failures of aluminum wire connections in residential circuits, Anal. Chem., 1982, 54(9), p A059-A064.
[18] E. Kandare, S. Feih, A. Kootsookos, Z. Mathys, B.Y. Lattimer, A.P. Mouritz, Creep-based life prediction modelling of aluminium in fire, Mater. Sci. Eng. A, 2010, 527(4-5), p 1185-1193.
[19] F.J. Humphreys, Review - Grain and subgrain characterisation by electron backscatter diffraction,

J. Mater. Sci., 2001, 36(16), p 3833-3854.
[20] C.J. Shi, W.M. Mao, X.G. Chen, Evolution of activation energy during hot deformation of AA7150 aluminum alloy, Mater. Sci. Eng. A, 2013, 571, p 83-91.
[21] E. Orowan, Dislocation in metals, AIME, New York, M. Cohen(Ed), 1957, p 103-131.
[22] E. Arzt, D.S. Wilkinson, Threshold stresses for dislocation climb over hard particles - the effect of an attractive interaction, Acta Metall., 1986, 34(10), p 1893-1898.
[23] E. Arzt, J. Rosler, The kinetics of dislocation climb over hard particles .2. Effects of an attractive particle dislocation interaction, Acta Metall., 1988, 36(4), p 1053-1060.
[24] R.A. Karnesky, L. Meng, D.C. Dunand, Strengthening mechanisms in aluminum containing coherent Al_3Sc precipitates and incoherent Al_2O_3 dispersoids, Acta Mater., 2007, 55(4), p 1299-1308.
[25] Y. Li, T.G. Langdon, An examination of a substructure-invariant model for the creep of metal matrix composites, Mater. Sci. Eng. A, 1999, 265(1-2), p 276-284.
[26] F. Dobes, P. Kratochvil, The effect of Zr addition on creep of Fe-30 at.% Al alloys, Intermetallics, 2013, 43, p 142-146.
[27] Z.G. Lin, F.A. Mohamed, Creep and microstructure in powder metallurgy 15 vol.% SiCp-2009 Al composite, J. Mater. Sci., 2012, 47(6), p 2975-2984.
[28] J.E. Dorn, N. Jaffe, Effect of temperature on the creep of polycrystalline aluminum by the cross-slip mechanism, Trans. Met. Soc. AIME, 1961, 221(2), p 229-233.
[29] N. Jaffe, J.E. Dorn, Effect of stress on creep Rate of high-purity aluminum in cross-slip region, Trans. Met. Soc. AIME, 1962, 224(6), p 1167-1173.
[30] O. Ryen, O. Nijs, E. Sjolander, B. Holmedal, H.E. Ekstrom, E. Nes, Strengthening mechanisms in solid solution aluminum alloys, Metall. Mater. Trans. A, 2006, 37A(6), p 1999-2006.
[31] P.K. Chaudhury, F.A. Mohamed, Creep and ductility in an Al-Cu solid-solution alloy, Metall. Mater. Trans. A, 1987, 18(12), p 2105-2114.
[32] V.K. Rao, D.M.R. Taplin, P.R. Rao, The grain size dependence of flow and fracture in a Cr-Mn-N austenitic steel from 300 to 1300K, Metall. Trans. A, 1975, 6A(1), p 77-86.

Table

Table 1 Chemical composition of experimental alloys studied (wt.%)

Alloy	Fe	Cu	Mg	Si	Mn	Al
Al3 (0.3Fe)	0.3	0.18	0.001	0.023	0.0003	Bal.
Al5 (0.5Fe)	0.5	0.17	0.001	0.027	0.0004	Bal.
Al7 (0.7Fe)	0.7	0.19	0.001	0.042	0.0006	Bal.

Figures

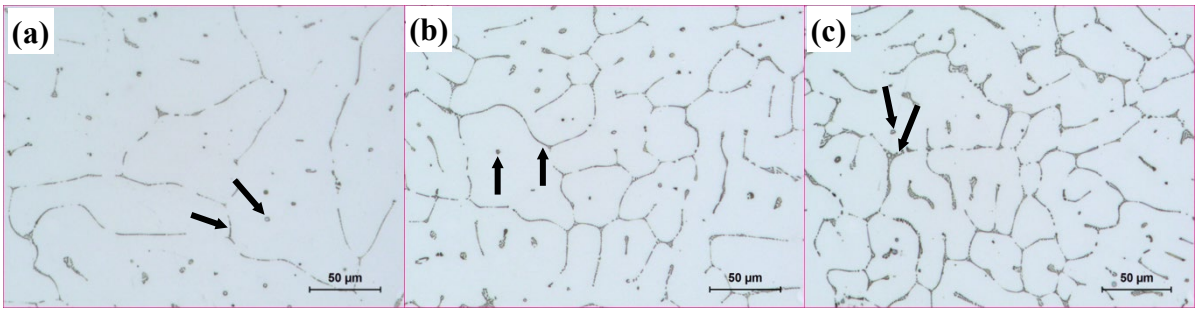

Fig. 1 Optical micrographs showing the as-cast grain structures: (a) Al3; (b) Al5; (c) Al7

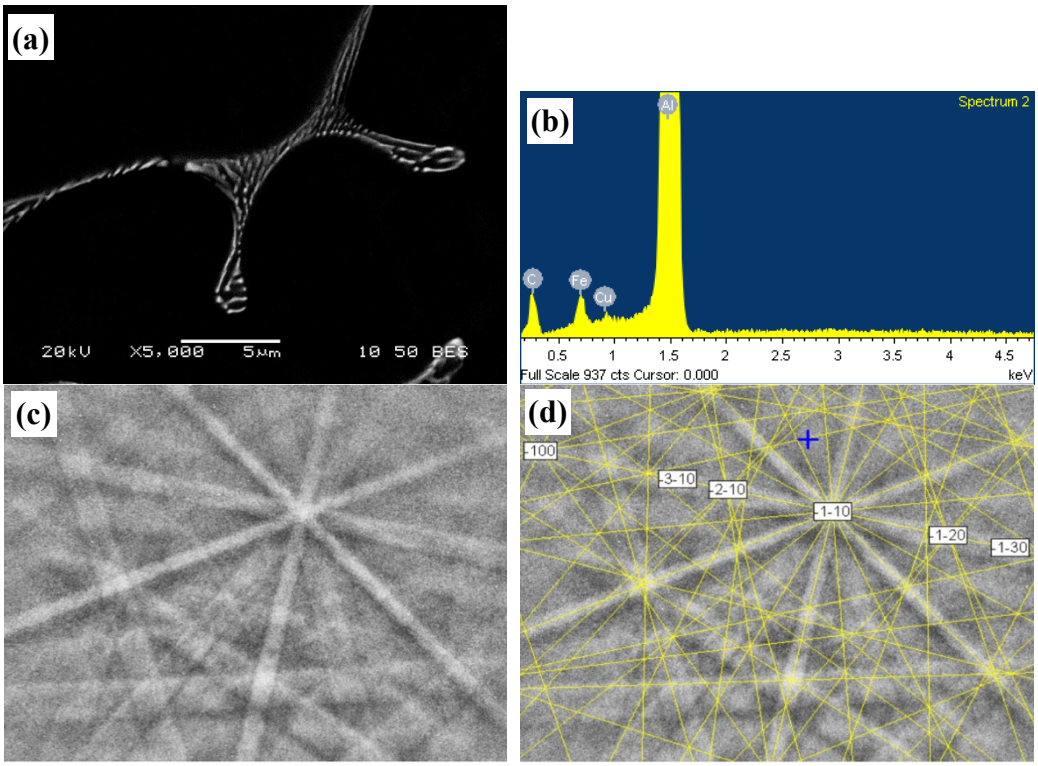

Fig. 2 Typical characteristics of Fe-rich intermetallics in Fig. 1: (a) SEM micrograph; (b) EDS spectrum; (c) EBSD pattern; (d) simulated solution of EBSD pattern, identifying Al_mFe phase with a lower mean angular deviation of 0.315

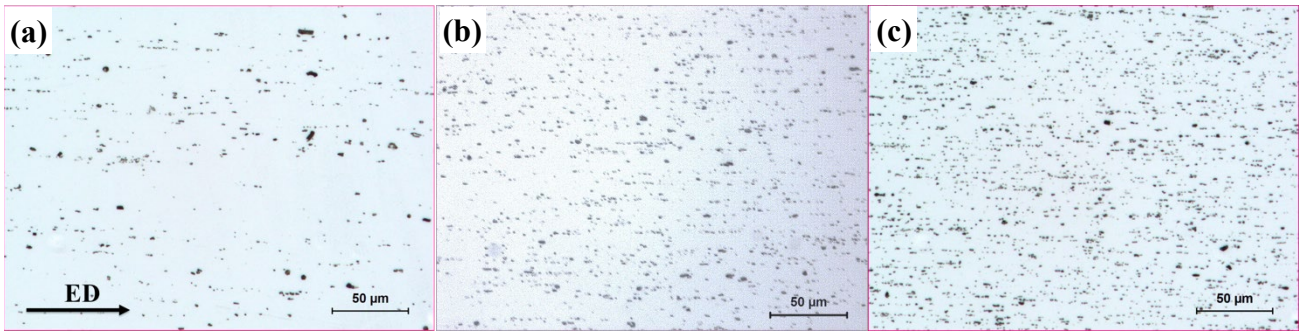

Fig. 3 Optical micrographs of the extruded samples: (a) Al3; (b) Al5; (c) Al7, showing fine Fe-rich intermetallic particles distributed along the extrusion direction (ED)

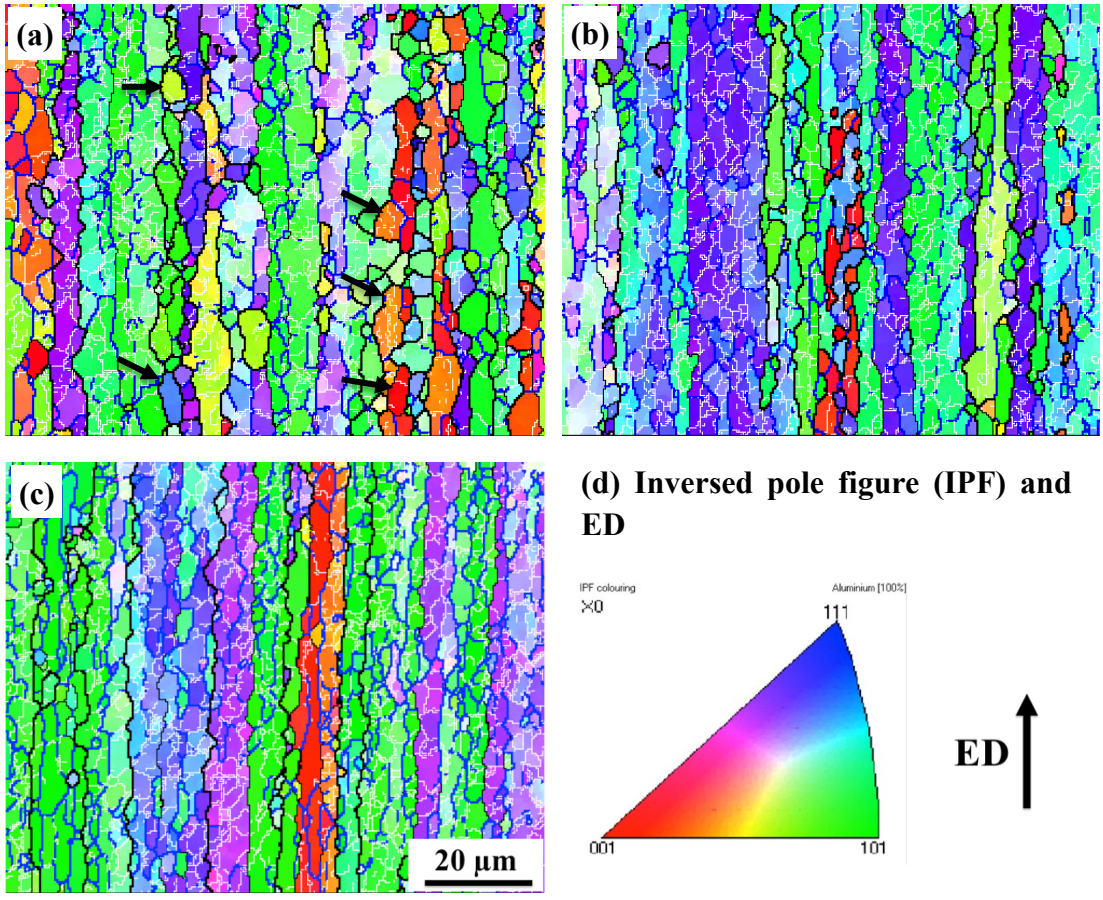

Fig. 4 Orientation imaging maps of the extruded samples with different Fe contents: (a) Al3; (b) Al5; (c) Al7; (d) Inversed pole figure (IPF) and extrusion direction (ED)

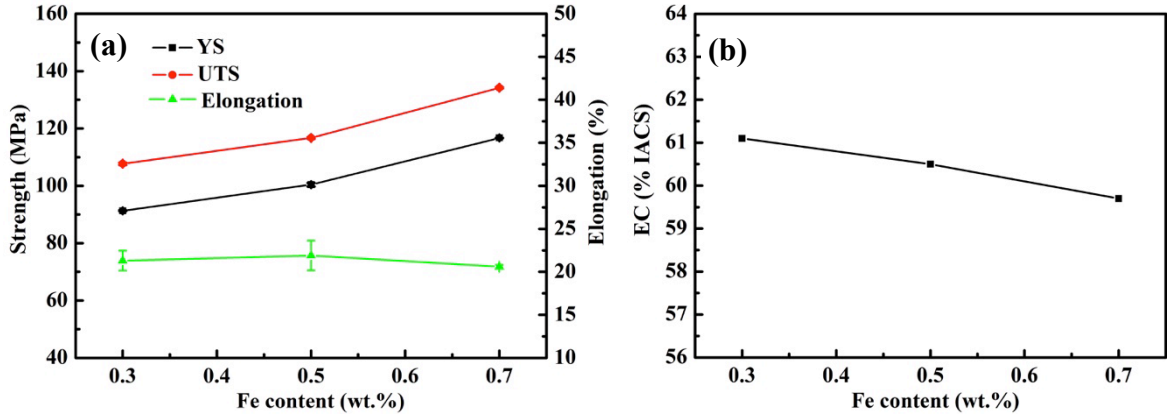

Fig. 5 Evolution of mechanical properties (a) and EC (b) with different Fe contents

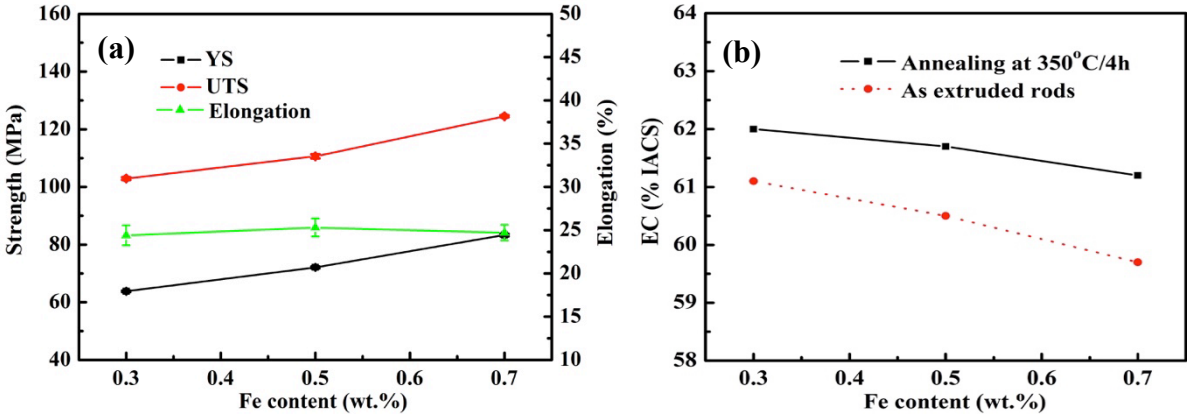

Fig. 6 Mechanical properties (a) and EC (b) of the samples after annealing at 350 ºC for 4 h

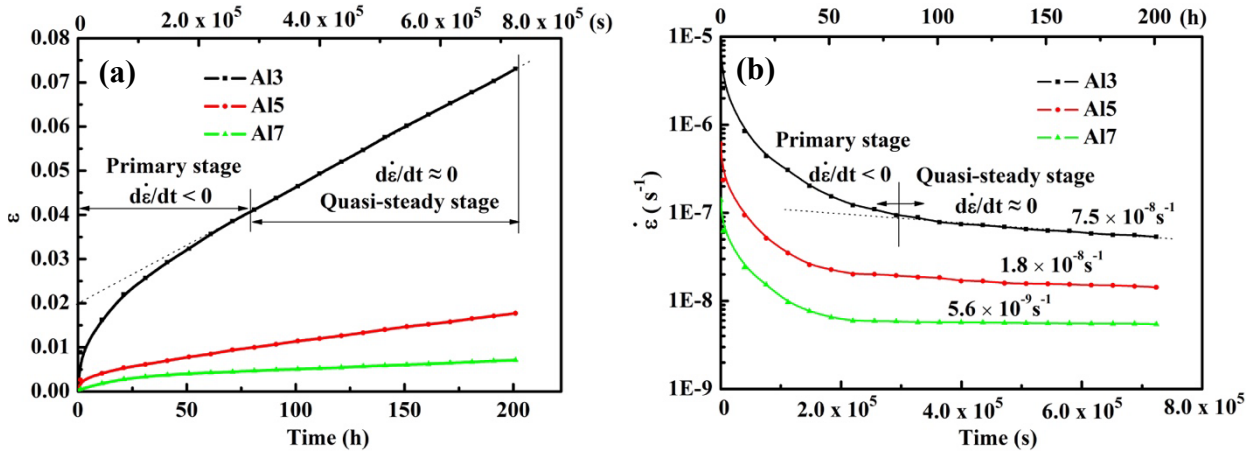

Fig. 7 Typical creep strain (ε) (a) and instantaneous creep rate ($\dot{\varepsilon}$) (b) curves of the samples with different Fe contents, tested at 100°C and 69 MPa

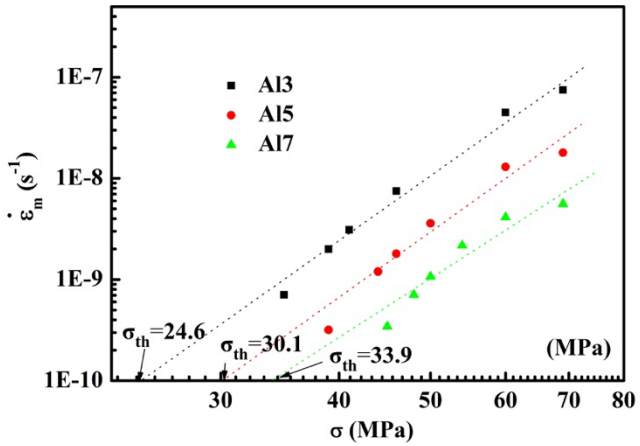

Fig. 8 Double logarithmic plot of the minimum creep rate $\dot{\varepsilon}_m$ against applied stress σ for Al3, Al5, and Al7 alloys

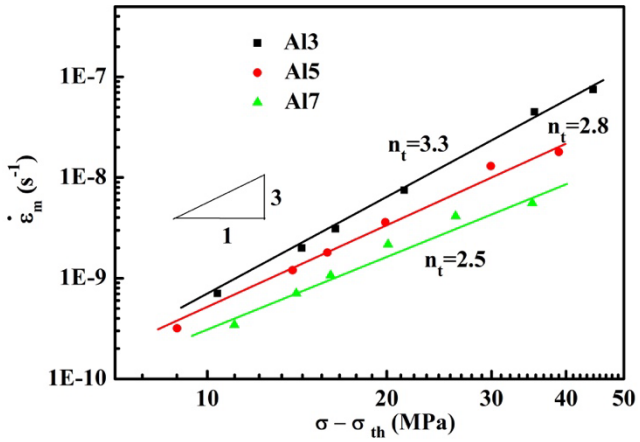

Fig. 9 Double logarithmic plot of minimum creep rate $\dot{\varepsilon}_m$ vs effective stress $\sigma - \sigma_{th}$ for Al3, Al5 and Al7 alloys

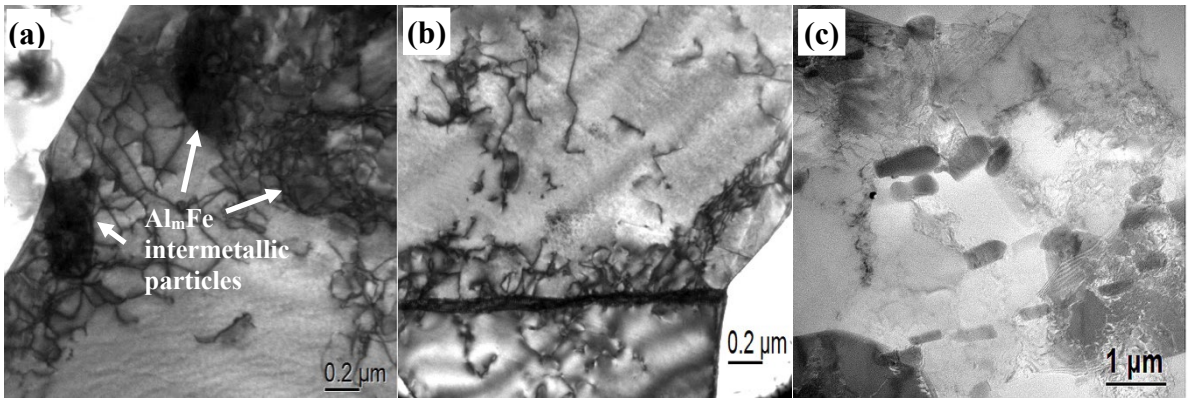

Fig. 10 TEM bright field images of Al3 samples after creep at 100°C and 69 MPa, representing interaction between dislocations and dispersion particles: (a) dislocation pile-up at Al_mFe intermetallic particles, (b) subgrain boundary blocking the dislocation motion, and (c) intermetallic particles

distributed on subgrain boundaries

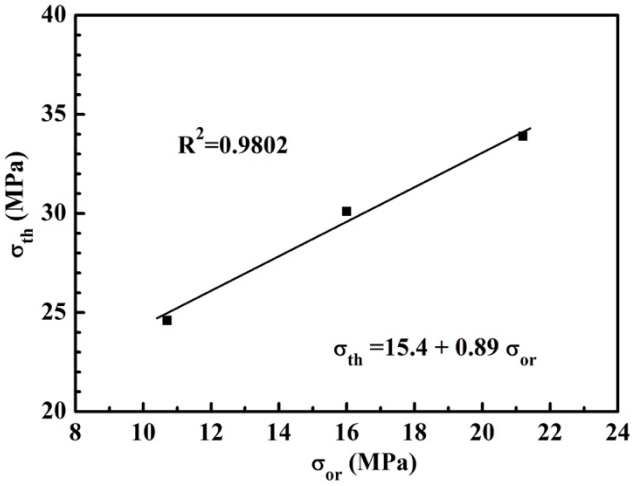

Fig. 11 Relation between the threshold stress, σ_{th} and Orowan stress, σ_{or}